Journal Name

ARTICLE TYPE

Cite this: DOI: 00.0000/xxxxxxxxxx

Supplementary Materials: Investigating magnetostatics of Fe–Ni nanosphere assemblies by electron holography and micromagnetic simulations†

Yanlong Li,[a] Shuhang Liao,[a] Xianhui Ye,[a] Jiaqi Su,[a] and Zi-An Li*[a]

Received Date
Accepted Date

DOI: 00.0000/xxxxxxxxxx

[a] School of Physical Science and Technology, Guangxi University, Nanning 530004, China. E-mail: zianli@gxu.edu.cn

† Supplementary Information available.

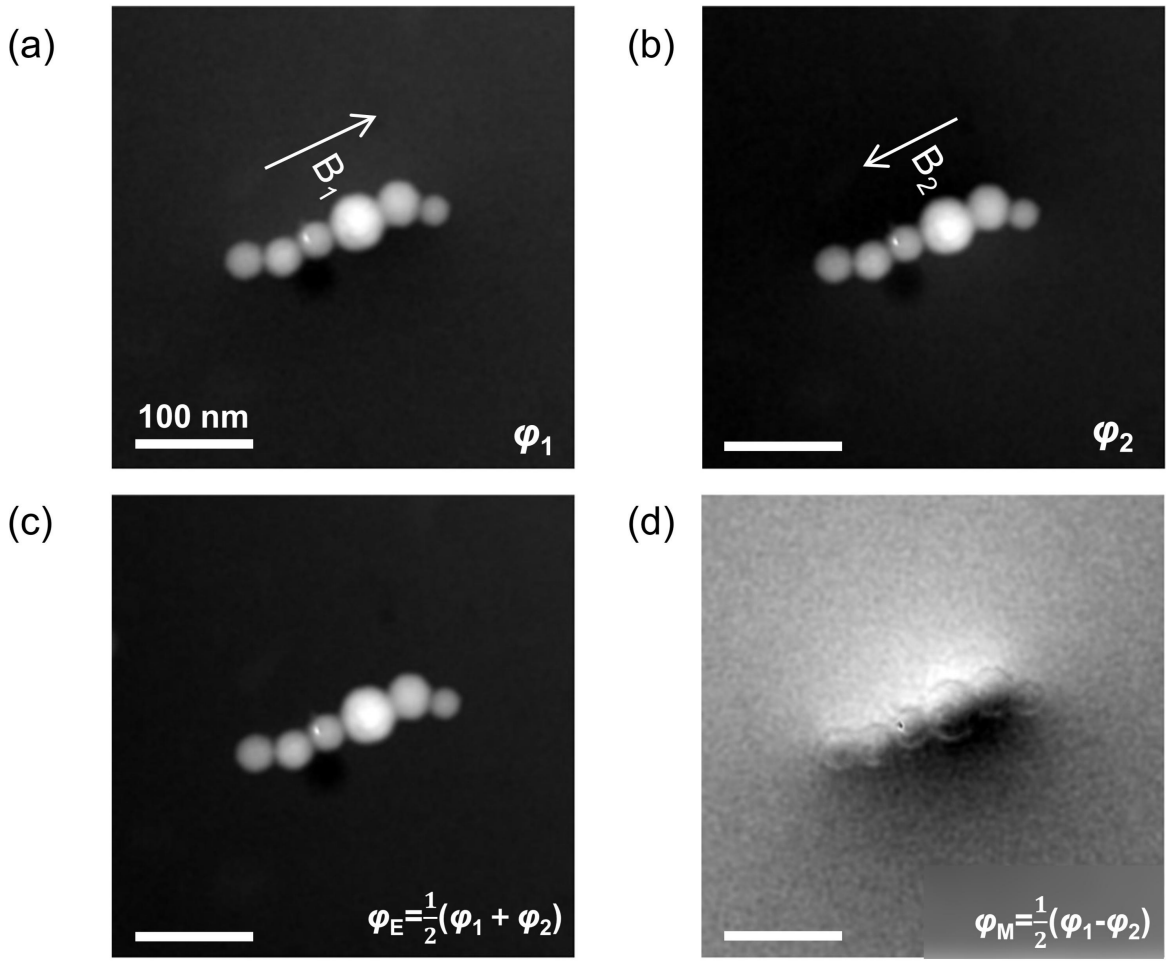

Fig. S1 Separation of the electrostatic and magnetic phase contributions for a $Fe_{30}Ni_{70}$ nanosphere chain. (a, b) Reconstructed holographic phase images acquired after magnetizing the sample in opposite directions. (c) The electrostatic (mean inner potential) phase image, obtained by calculating half the sum of the phase images in (a) and (b). (d) The purely magnetic phase image, obtained by calculating half the difference between the phase images in (a) and (b).

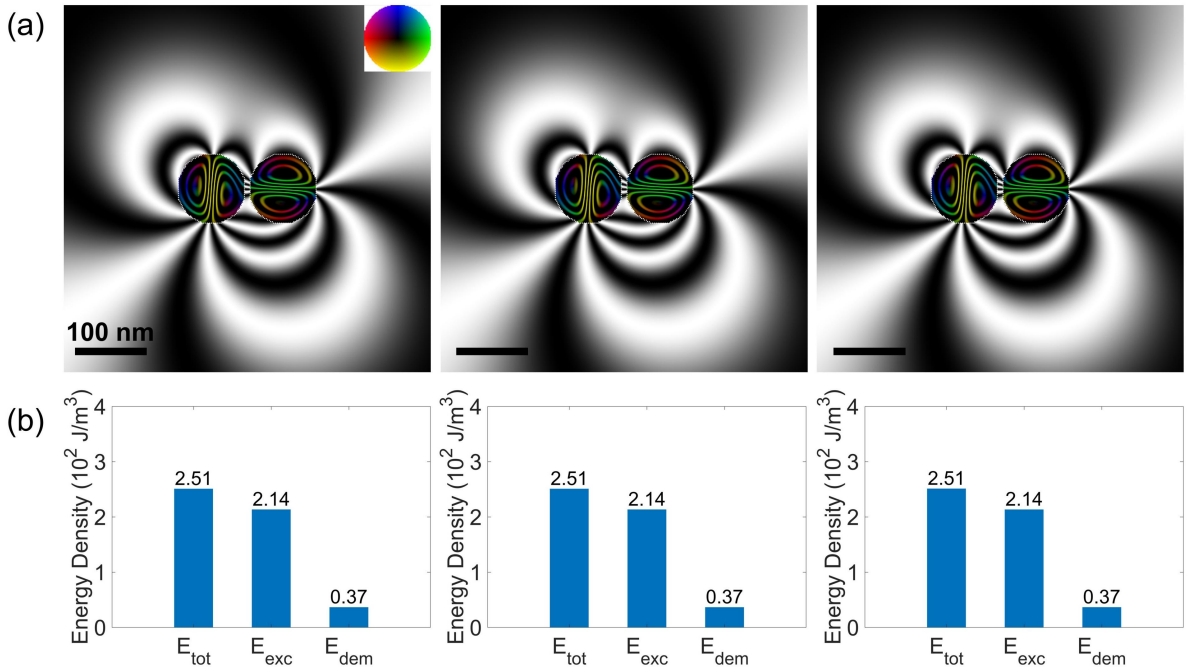

Fig. S2 Sensitivity test of cubic magnetocrystalline anisotropy-axis settings for a 94 nm $Fe_{30}Ni_{70}$ dimer. (a) Simulated magnetic phase contour maps for three representative anisotropy-axis settings, shown from left to right: $[100] \parallel x$, $[010] \parallel y$, $[001] \parallel z$; $[100] \parallel z$, $[010] \parallel y$, $[001] \parallel x$; and crystal $[111] \parallel z_{\mathrm{sim}}$. The relaxed magnetic phase distributions are nearly identical in the three cases, and all exhibit non-collinear vortex-core configurations. (b) Corresponding energy-density terms for the three anisotropy-axis settings, shown in the same left-to-right order as in (a). The demagnetization, exchange, and total energy densities remain essentially unchanged among the three cases, and the total energy density is mainly determined by the sum of the exchange and demagnetization contributions.

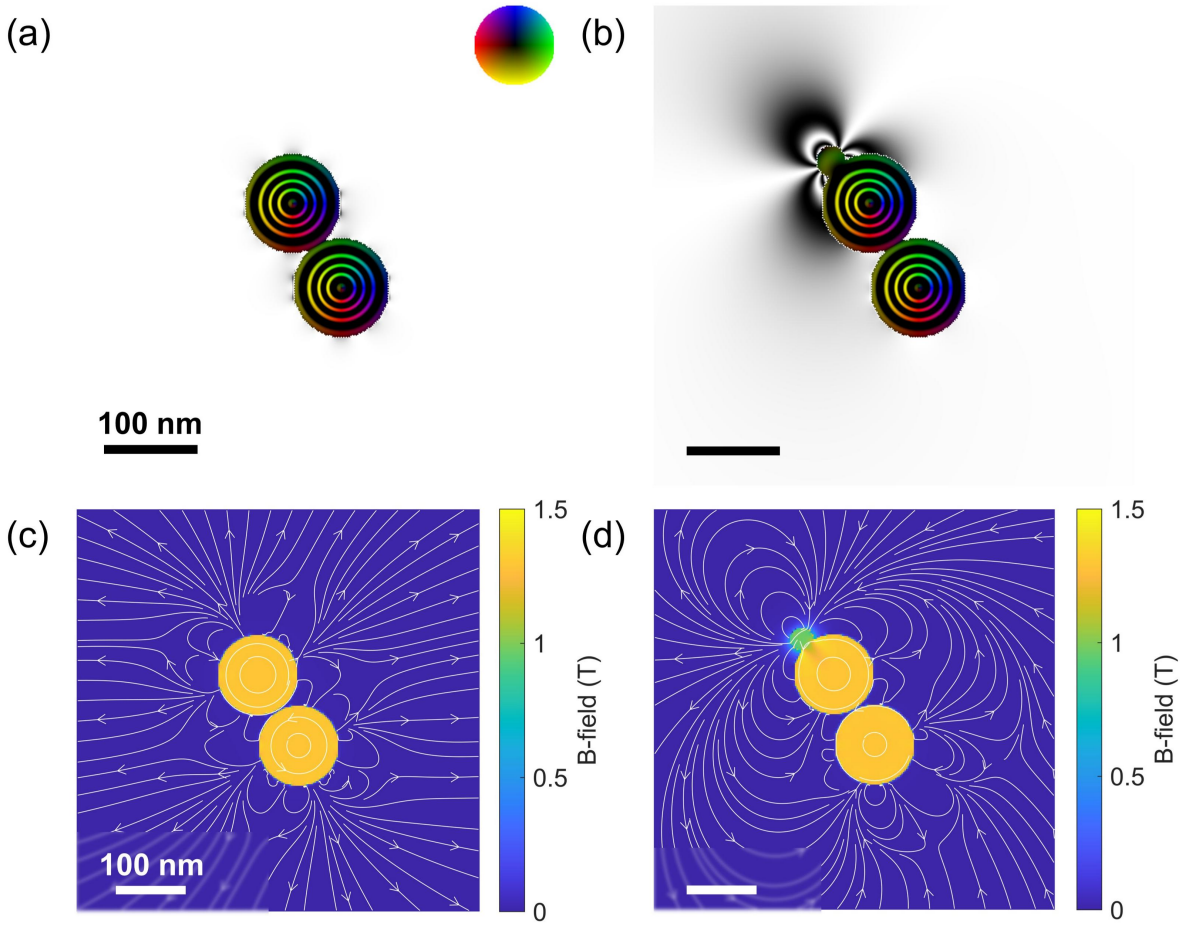

Fig. S3 Control simulations for evaluating the influence of the small neighboring nanosphere on the vortex-core configuration of the large $Fe_{30}Ni_{70}$ dimer. (a) Simulated magnetic phase contour map of an idealized dimer consisting of two 102 nm $Fe_{30}Ni_{70}$ nanospheres. The two large particles relax to a non-collinear vortex-core configuration. (b) Simulated magnetic phase contour map of a three-particle model consisting of the same two 102 nm nanospheres and an additional ∼30 nm neighboring nanosphere, following the experimental morphology in Figure **??**b. The two large particles still exhibit a non-collinear vortex-core configuration. (c,d) Corresponding magnetic field distributions for the two-particle dimer and the three-particle model, respectively. The comparison shows that the non-collinear vortex-core configuration of the large dimer is not induced by the small neighboring particle, although the latter may introduce a local perturbation to the surrounding magnetic field.

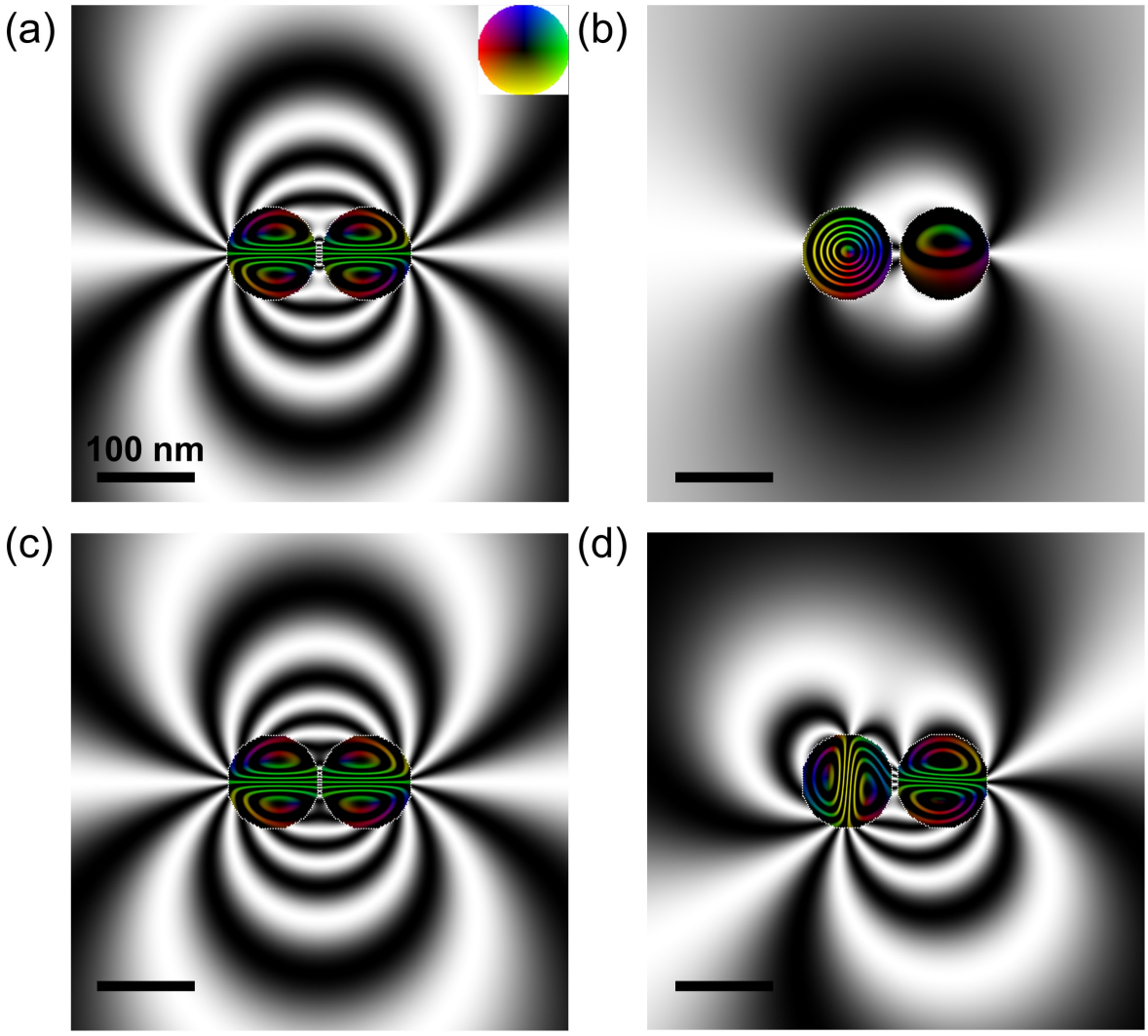

Fig. S4 Spacing-dependent simulations of $Fe_{30}Ni_{70}$ dimers near the critical transition between collinear and non-collinear vortex-core configurations. Simulated magnetic phase contour maps are shown for dimers with different particle diameters and edge-to-edge spacings: (a) a 92 nm dimer with a 6 nm spacing, showing a collinear vortex-core configuration; (b) a 92 nm dimer with an 8 nm spacing, showing a non-collinear configuration; (c) a 94 nm dimer with a 2 nm spacing, showing a collinear configuration; (d) a 94 nm dimer with a 4 nm spacing, showing a non-collinear configuration.